

4

PNe Flux Determinations

4.1 Method

For narrow-band images the total flux detected is reduced by the transmission of the H α and [O III] filters. This and other factors must be taken into account when determining actual flux values, and I now describe the methods used to arrive at the values listed in Table 4.1.

The central position of each object was computed by fitting a Gaussian to the image distribution and then the magnitude was calculated by integrating over successively larger diameters of the central area. By plotting these radii against magnitude it was possible to determine the radius at which the flux level matched that of the background continuum (see example in Fig. 4.1), and therefore the total flux of the object in ADU counts per 30 second exposure. These profiles were compared with those of standard stars LTT1020 and LTT624 to determine the aperture correction.

To determine detector flux values in mW m^{-2} ($\text{erg cm}^{-2}\text{s}^{-1}$), the ratio of ADU count to flux conversion factor was calculated by measuring the count in ADUs per ten seconds of LTT1020 and LTT6248, and comparing it with tabulated fluxes for these spectrophotometric standards (Hamuy et al. 1994). The calibration counts were factored for the shorter exposure time, and an aperture correction of -5 per cent was applied. Apart

4: PNE FLUX DETERMINATIONS

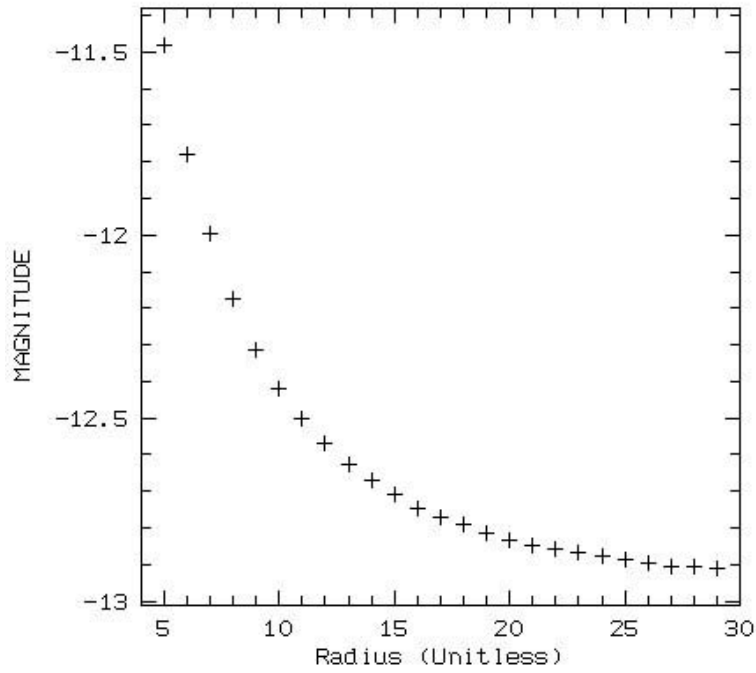


Figure 4.1: Determination of maximum $H\alpha$ flux level from PN radius, where flux level matches that of the background continuum, for M2-10 (PN G 354.2+04.3).

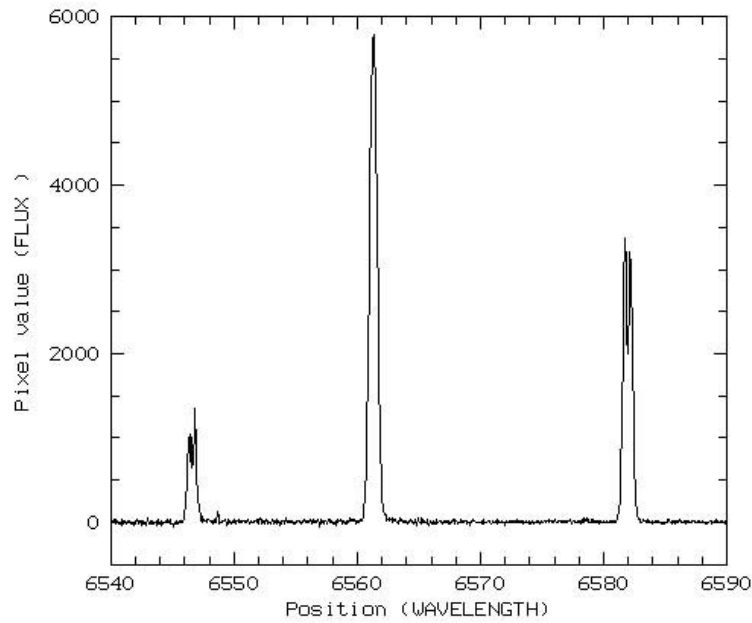


Figure 4.2: Example of $[N II]$ contribution to $H\alpha$ flux. $H\alpha$ line at 6565 Å and $[N II]$ lines at 6548 Å and 6584 Å (rest wavelengths) for M2-10 (PN G 354.2+04.3).

from a brief period of non-photometric conditions caused by cloud (indicated as ‘npc’ in Table 4.1), observations were considered photometric as the computed ADU count to flux ratios varied by no more than 2.1 per cent between the two night’s observations.

In order to determine actual H α 6565 Å flux values, any contribution from [N II] lines at 6548 Å and 6584 Å (vacuum), passing through ESO filter #654, needed to be taken into account (see example in Fig. 4.2). This was done by assuming the following expression for the total detected flux:

$$F_{\text{det}} = F_{6565}T_{6565} + F_{6584}T_{6584} + F_{6548}T_{6548} \quad (4.1)$$

where $F\lambda$ and $T\lambda$ are actual flux values and filter transmission coefficients (corrected for the appropriate Doppler shift – see below) respectively. Using catalogue [N II] to H α flux ratios $R_{6584} = F_{6584}/F_{6565}$ and $R_{6548} = F_{6548}/F_{6565}$ (which avoid a dependence on absolute values), the actual H α 6565 Å flux can be calculated using:

$$F(\text{H}\alpha)_{\text{obs}} = F_{\text{det}}/(T_{6565} + R_{6584}T_{6584} + R_{6548}T_{6548}) \quad (4.2)$$

[N II]₆₅₄₈ flux values were calculated from the [N II]₆₅₈₄ catalogue values (Acker et al. 1992) using a factor of 2.97 (Cox 2000). In the case of [O III], the flux observed through the filter was factored for the appropriate transmission coefficient of the [O III] wavelength, so as to arrive at actual observed [O III] flux values.

The H α and [O III] wavelengths, λ_T , observed at the telescope are Doppler shifted relative to the emitted wavelengths, λ_0 , due to the source’s radial velocity, v_r , relative to the Sun, and the telescope’s barycentric velocity, v_b , due to the Earth’s rotational motion, and orbital motion around the Sun. The former calculation is simply $\Delta\lambda = v_r\lambda_0/c$, but the latter involves a barycentric calculation that takes into account the date and time at La Silla, and therefore the telescope’s motion with respect to the centre of mass of the Solar system (as opposed to a heliocentric correction based solely on the Sun’s position). Therefore, the shift in wavelength at the telescope, $\Delta\lambda_T$, is given by

$$\Delta\lambda_T = \lambda_a(v_r - v_b)/c, \quad (4.3)$$

4: PNE FLUX DETERMINATIONS

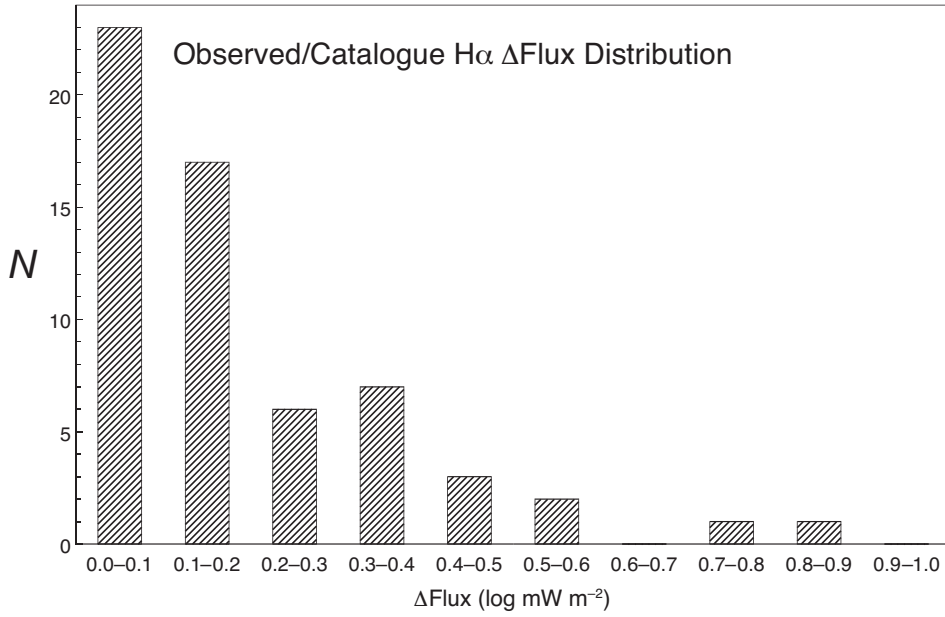


Figure 4.3: Distribution of $\Delta F(\text{H}\alpha)$, the absolute difference between observed and catalogued $\text{H}\alpha$ flux values ($\log \text{mW m}^{-2}$).

where λ_a is the air wavelength at the telescope and c is the speed of light. Fortunately, ESO's MIDAS software includes a routine for this calculation that utilises time and date information in the FITS header of each image file (ESO 1998a). Therefore, the Doppler shifted $\text{H}\alpha$ and $[\text{O III}]$ wavelengths observed at the telescope were computed from catalogue radial velocities (Durand et al. 1998; Acker et al. 1992) less the barycentric correction, or in the absence of a catalogue value, derived from spectra taken during the observations. For receding objects, positive v_r produces a redward shift in λ , whereas approaching objects with negative v_r are blue shifted.

Columns four and five of Table 4.1 compare catalogue radial velocities with observed values, which I consider accurate to $\pm 25 \text{ km s}^{-1}$. For four objects it was not possible to determine the radial velocity at all (283.8+02.2, My60; 296.4-06.9, He2-71; 305.1+01.4, He2-90; 352.6+00.1, H1-12). Using the corrected filter response curves (measured at La Silla air pressure), the appropriate transmission coefficient was then applied to arrive at actual flux values. La Silla-air wavelengths were 6563.3 Å for $\text{H}\alpha$ and 5007.3 Å for $[\text{O III}]$, with 6548.5 Å and 6583.9 Å assumed for $[\text{N II}]$ using the same

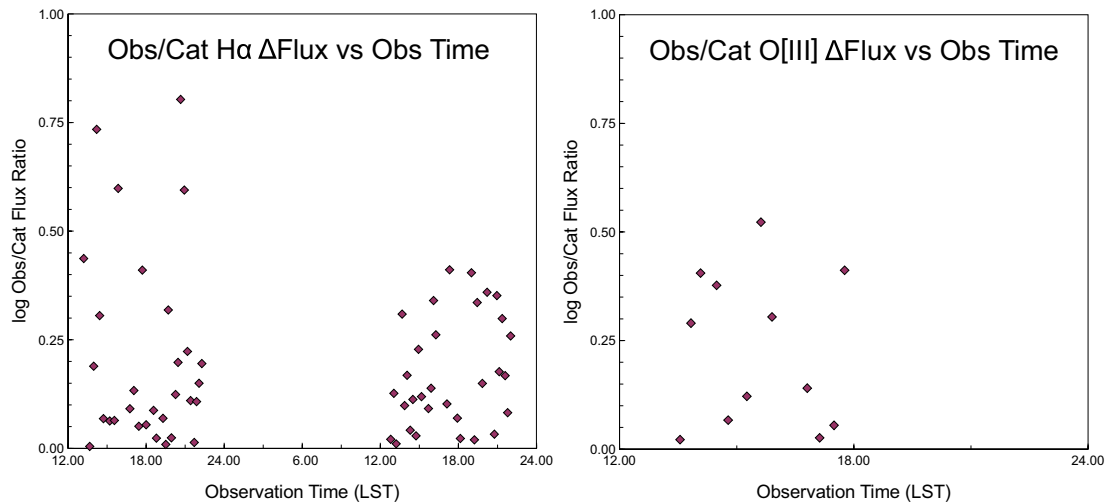


Figure 4.4: Comparison of ΔF ($H\alpha$ and $[O III]$), the absolute difference between observed and catalogued flux values ($\log \text{mW m}^{-2}$) with observation time (LST).

$\Delta\lambda$ as that of $H\alpha$. Although stellar velocities in the Bulge are typically of the order of $\pm 100 \text{ km s}^{-1}$ (Minniti 1996), or about $\pm 2 \text{ \AA}$, I chose to calculate precise Doppler wavelength shifts, in order to take into account the sensitivity of the $H\alpha$ filter transmission curve to small changes in observed wavelength.

I was able to compare some of my initial flux determinations with more recent PNe data obtained from the Hubble Space Telescope (HST) by Zijlstra (2004). Certain differences led me to investigate the accuracy of the $H\alpha$ on-band filter response curve that had been obtained from ESO (this is explained in more detail in section 2.3). After making corrections for the actual $H\alpha$ on-band filter response curve and the position of the PN image on the CCD array, my flux determinations agreed with the HST values within my margin of error, and the spread of $\Delta F(H\alpha)$ between observed and catalogued $H\alpha$ flux values was reduced. Subsequent investigation (Zijlstra 2005) suggests that these filters have deteriorated over time. For this reason I would recommended always taking calibration spectra from the optical centre of the field to determine filter response data.

4: PNE FLUX DETERMINATIONS

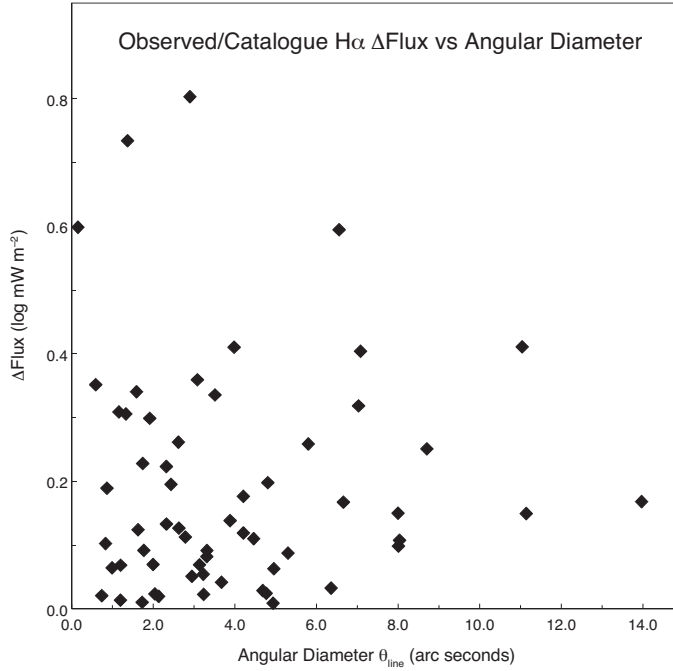


Figure 4.5: Comparison of $\Delta F(H\alpha)$ the absolute difference between observed and catalogued $H\alpha$ flux values ($\log \text{mW m}^{-2}$) with angular diameter θ_{line} .

4.2 Results and error factors

Table 4.1 lists the newly determined $H\alpha$ and $[O \text{ III}]$ flux densities in column six. For comparison columns seven and eight list $H\alpha$ and $[O \text{ III}]$ flux values (calculated from catalogued $H\beta$ flux and line intensities) and the 6 cm radio flux values from the Strasbourg – ESO Catalogue (Acker et al. 1992). Radio values in bold are for the two PNe in the Sagittarius dwarf galaxy (from Dudziak et al. 2000). Fig. 4.3 shows the distribution of $\Delta F(H\alpha)$, the absolute difference between observed and catalogued $H\alpha$ flux values. 7 out of 60 objects are shown to have $\Delta F(H\alpha) > 0.4$ ($\log \text{mW m}^{-2}$). Fig. 4.4 shows little evidence of a correlation between $\Delta F(H\alpha)$ and $[O \text{ III}]$ with observation time (LST), although there were brief periods of non-photometric conditions on the first night, which appears to be reflected in the bigger spread of $\Delta F(H\alpha)$ for the first night. Figs. 4.5, 4.6 and 4.7 show no evidence of a correlation between $\Delta F(H\alpha)$ and angular diameter θ_{line} , $H\alpha$ filter transmission coefficient, or radial velocity.

Fig. 4.8 compares observed and catalogued $H\alpha$ and $[O \text{ III}]$ flux values. Four (non-

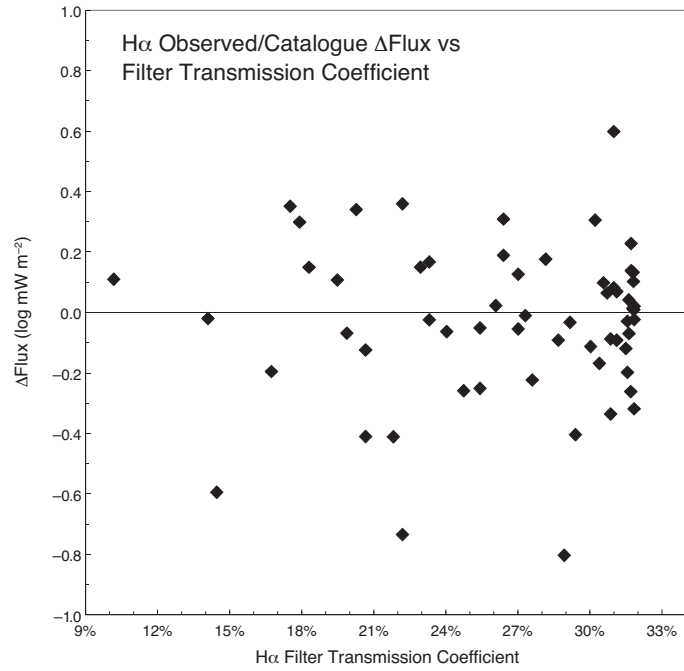


Figure 4.6: Comparison of $\Delta F(H\alpha)$ the absolute difference between observed and catalogued $H\alpha$ flux values ($\log \text{mW m}^{-2}$) with $H\alpha$ filter transmission coefficient.

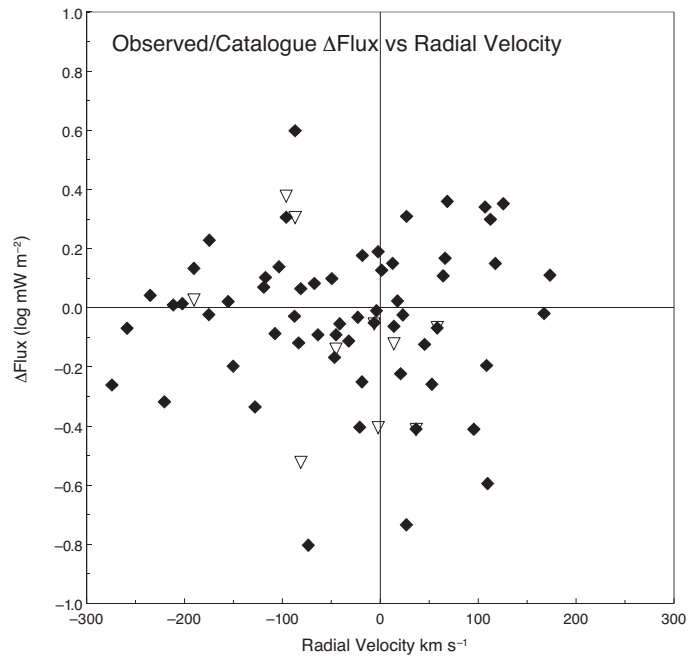


Figure 4.7: Comparison of $\Delta F(H\alpha)$ the absolute difference between observed and catalogued $H\alpha$ flux values ($\log \text{mW m}^{-2}$) with radial velocity (km s^{-1}).

4: PNE FLUX DETERMINATIONS

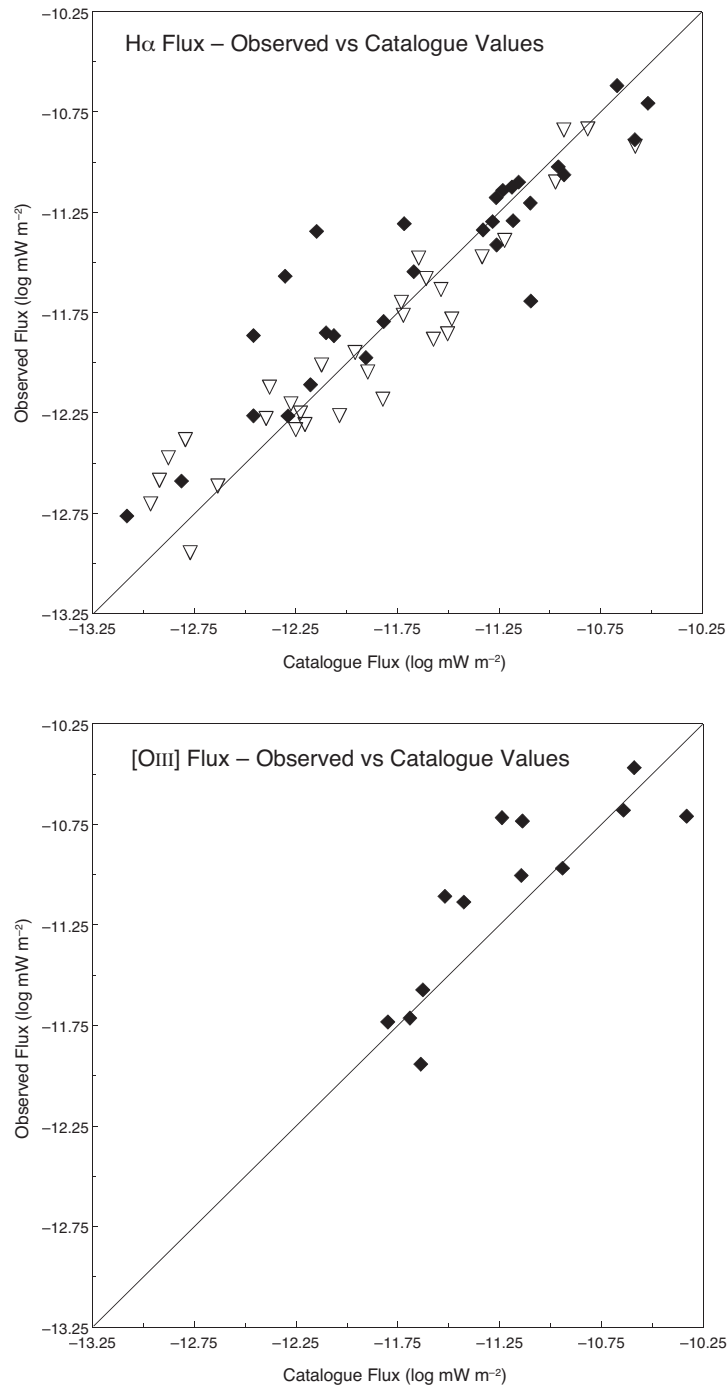


Figure 4.8: Comparison of observed and catalogued H α and [O III] flux values (log mW m⁻²). Diamonds denote objects observed on the first night, triangles the second.

Bulge) objects (indicated in Table 4.1) are excluded from Figs. 4.3 and 4.8 because atmospheric conditions for those exposures were non-photometric. It can be seen that there is little evidence of any systematic differences between observed and catalogued flux values. For [O III] there is a tendency to higher observed flux values at intermediate flux densities. However, this may not be significant as the [O III] sample is small compared to the H α sample.

Possible sources of error in my flux determinations are: poor photometry; residual stellar background flux after subtraction of the continuum; an off-centred peak in the H α on-band filter response curve; estimation of the flux contribution from [N II] lines; the accuracy of transmission coefficients in the corrected filter response tables (particularly for H α); change in passbands of filters due to their age, input beam and ambient temperature; integrating the transmission profile of the filter response curves; uncertainties in radial velocities; changes in air pressure (airmass); and the aperture correction factor of 5 per cent. Of these, I consider the accuracy of the filter response data the most significant and therefore suggest an error factor in the calculated flux values (mW m^{-2}) of ± 5 per cent for blue-shifted objects and ± 10 per cent for red-shifted objects.

Table 4.1: Flux and extinction values of 70 planetary nebulae. Observed H α extinction (equation 5.14) and catalogue H α extinction (equation 5.20), R_V (equation 5.24) and ΔR_V (equation 5.28) are defined in section 5.

PN G	Object	Line	Radial Vel. (km s ⁻¹)		Flux (log mW m ⁻²)		Sv 6 cm (mJy) [†]	H α Extinction		R_V	ΔR_V	Notes ⁵
			Observed	Catalogue	Observed	Catalogue		Observed	Catalogue			
000.3-04.6	M2-28	H α	-43.5	-29.9	-11.70	-11.73	10	0.66	0.98	1.99	0.62	B
000.3-02.8	M3-47	H α	-17.9	-16.0	-12.47	-12.88			1.58			
000.6-01.3	B13-15	H α	-114.8		-12.59	-12.92			2.89			
000.8-01.5	B10	H α	79.9		-12.18	-11.82			2.04			
002.3-03.4	H2-37	H α	-129.8	-156.8	-11.86	-12.06			0.69			
002.8-02.2	Pe2-12	H α	108.8		-11.86	-12.46	2	0.13	1.06	0.57	0.41	lrf
003.0-02.6	KFL4	H α	-12.9	17.0	-12.59	-12.81	1	0.59	1.02	1.71	0.56	lrf
003.6+03.1	M2-14	H α	-25.0	-48.2	-11.35	-12.15	39	0.90	1.41	1.87	0.42	B
003.7-04.6	M2-30	H α	130.0	154.9	-11.29	-11.18	14	0.40	0.74	1.59	0.75	B
003.8-17.1	Hb8	H α	-170.1	-180.5	-11.30	-11.28	6	0.03	0.20	0.64	2.30	lrf
004.0-11.1	M3-29	H α	26.2	49.3	-11.20	-11.10	12	0.25	0.12	10.81	31.50	B
004.7-11.8	He2-418	H α	87.7	109.3	-12.05	-11.90			0.12			
004.8-22.7	He2-436	H α	128.4	133.0	-11.86	-11.50	3.9	0.41	0.50	2.45	1.36	lrf
004.8-05.0	M3-26	H α	-24.7	-9.8	-11.41	-11.26	8	0.28	0.43	1.90	1.40	lrf
005.2-18.6	StWr2-21	H α	136.3	133.0	-12.26	-12.46			0.32			
006.0-41.9	PRMG1	H α	-8.1		-12.95	-12.77			0.18			
006.8-19.8	Wray16-423	H α	139.2	133.0	-11.78	-11.48	4.7	0.42	0.36	3.78	2.47	lrf
008.6-07.0	He2-406	H α	-8.5	28.2	-12.12	-12.38			0.84			
008.6-02.6	MaC1-11	H α	-30.8	-89.0	-12.33	-12.25			1.76			
009.4-09.8	M3-32	H α	40.1	58.4	-11.39	-11.22	12	0.43	0.53	2.46	1.29	B
009.8-07.5	GJJC1	[OIII]		-32.0	-12.74							

PN G	Object	Line	Radial Vel. (km s^{-1})		Flux ($\log \text{mW m}^{-2}$)		Sv 6 cm (mJy) ⁴	H α Extinction		R_V	ΔR_V	Notes ⁵
			Observed	Catalogue	Observed	Catalogue		Observed	Catalogue			
037.5-05.1	A58	H α		70.0	-13.40							
		[OIII]			-12.91							
283.8+02.2	My60	H α			≥ -11.53	-11.04	60	≤ 1.27	0.67			npc
		[OIII]			≥ -10.68	-10.64						
289.8+07.7	He2-63	H α		123.2	≥ -11.92	-11.91	12	≤ 0.96	0.27			npc
		[OIII]			≥ -11.14	-11.43						
292.8+01.1	He2-67	H α		59.5	≥ -12.47	-11.17	41	≤ 1.51	0.83			npc
296.4-06.9	He2-71	[OIII]			≥ -11.71	-11.69						npc
305.1+01.4	He2-90	H α			≥ -10.71	-10.52	25		1.13			hbt
		[OIII]			≥ -10.73	-11.14						
315.4+09.4	He2-104	H α	-70.4	-143.6	-10.83	-10.81	<15		1.09			hbt
321.3-16.7	He2-185	H α	-12.0	-6.0	-11.10	-10.97	18	0.32	0.20	6.24	7.24	
322.4-00.1	Pe2-8	H α	-23.9	-16.3	-11.95	-11.96	100	≥ 1.91	3.16	1.78	0.18	hbt
345.0-04.9	Cn1-3	H α	-68.2	-79.8	≥ -10.89	-10.58			0.13			npc
		[OIII]			≥ -10.71	-10.33						npc
345.0+03.4	Vd1-4	H α	93.4	35.1	-12.11	-12.18			0.84			
		[OIII]			-11.73	-11.80						
345.0+04.3	Vd1-2	H α		3.4	-11.57	-12.30			1.16			
		[OIII]			-13.08							
346.0+08.5	He2-171	H α	-100.2	-101.5	≥ -11.69	-11.09	10		1.54			hbt
		[OIII]			≥ -11.94	-11.64						

⁴ Bold values are for PNe in the Sagittarius dwarf galaxy (Dudziak et al. 2000). All other values from Acker et al. (1992).

⁵ B, Bulge subset B; npc, non-photometric conditions; hbt, high brightness temperature, $T_b > 10000 \text{ K}$; lrf, low radio flux, $S_y < 10 \text{ mJy}$.

Table 4.1 (continued): Flux and extinction values of 70 planetary nebulae.

PN G	Object	Line	Radial Vel. (km s ⁻¹) Observed Catalogue	Flux (log mW m ⁻²) Observed Catalogue	Sv 6 cm (mJy) [†]	H α Extinction Observed Catalogue	R _V	ΔR_V	Notes ⁵
346.3-06.8	Fg2	H α [OIII]	52.5 34.5	-11.12 -10.47	-11.19 -10.59	0.37			
347.4+05.8	H1-2	H α [OIII]	-124.8 -105.5	-11.02 -10.72	-10.96 -11.24	1.57	≥ 1.47	0.34	hbt
348.0+06.3	MGP1	H α	-67.9	-12.15	10.2	1.12			
348.8-09.0	He2-306	H α [OIII]	-49.6 -207.2	-11.14 -11.06	-11.23 -11.14	0.27			
349.8+04.4	M2-4	H α [OIII]	-227.0 -109.7	-11.06 -10.97	-10.93 -10.94	1.08	1.47	0.50	B
350.8-02.4	H1-22	H α	-199.6	-11.76	-11.72	1.66			
350.9+04.4	H2-1	H α [OIII]	-35.5 -18.8	-10.62 -11.57	-10.67 -11.63	0.79	1.38	0.67	B
351.1+04.8	M1-19	H α	-68.6	-11.10	-11.15	0.93	1.53	0.59	B
351.2+05.2	M2-5	H α	-134.6	-11.18	-11.26	0.90	0.84	0.52	B
351.3+07.6	H1-4	H α	10.1	-11.88	-11.57	0.52			
351.9-01.9	Wray16-286	H α	-143.9	-11.79	-11.82	1.91			
351.9+09.0	PC13	H α	-75.1	-11.63	-11.54	0.73			
352.0-04.6	H1-30	H α	5.6	-12.01	-12.12	1.30			
352.1+05.1	M2-8	H α [OIII]	18.2 25.1	-11.31 -11.11	-11.72 -11.52	0.78	1.99	0.79	B
352.6+00.1	H1-12	H α		-11.85	-12.10	3.88	2.02	0.16	

PN G	Object	Line	Radial Vel. (km s ⁻¹)		Flux (log mW m ⁻²)		S _ν 6 cm (mJy) [‡]	H α Extinction		R _V	ΔR_V	Notes ⁵
			Observed	Catalogue	Observed	Catalogue		Observed	Catalogue			
352.6+03.0	H1-8	H α	-3.9	-116.0	-11.97	-11.91		2.32				
352.8-00.2	H1-13	H α	-11.6	-26.3	-11.48	-11.65	> 620	2.23	2.60	2.59	0.27	
354.2+04.3	M2-10	H α	-64.2	-85.6	-11.58	-11.61	9.1	0.50	1.31	1.17	0.38	lrf
354.5+03.3	Th3-4	H α	-122.9	-165.0	-12.26	-12.03		2.15				
354.9+03.5	Th3-6	H α	-92.5	-73.1	-12.28	-12.40		1.93				
355.1-06.9	M3-21	H α	-78.6	-66.9	-10.84	-10.93	30	0.28	0.08	276.33	42.22	B
355.1+02.3	Th3-11	H α	-33.1		-12.81							
355.4-02.4	M3-14	H α	-63.3	-82.3	-11.47	-11.33	30	0.91	1.45	1.85	0.41	B
355.7-03.5	H1-35	H α	135.1	123.4	-10.92	-10.58	72	≥ 0.74	0.98	≥ 2.24	0.66	hbt
355.9+02.7	Th3-10	H α	-256.5		-12.70	-12.96	29.5	2.14	2.55	2.51	0.27	B
356.1+02.7	Th3-13	H α	-75.3	-99.0	-12.31	-12.20	14.3	≥ 1.43	2.69	≥ 1.56	0.21	hbt
356.8+03.3	Th3-12	H α	248.8	185.4	-12.61	-12.63	3.5	1.12	1.56	2.12	0.40	lrf
357.1-06.1	M3-50	H α	26.4	17.5	-12.26	-12.29			0.51			
357.1-04.7	H1-43	H α	44.9	49.0	-11.55	-11.67	6	0.29	0.93	0.99	0.52	lrf
357.1+01.9	Th3-24	H α	-152.4	-197.0	-12.76	-13.08		1.57				
357.1+03.6	M3-7	H α	-171.7	-193.6	-11.34	-11.33	28	0.75	1.20	1.84	0.49	B
357.6-03.3	H2-29	H α	123.4	107.0	-12.38	-12.79			1.30			
358.5+03.7	A12-B	H α	-134.0	-158.0	-12.97							
358.5-01.7	JaSt64	H α	17.6		-13.13							
358.7+05.2	M3-40	H α	54.0	32.8	-12.25	-12.23	15.1	1.39	1.93	2.13	0.33	B
359.2+04.7	Th3-14	H α	-206.7	-239.2	-12.20	-12.27	4	0.77	1.54	1.48	0.35	lrf

⁴ Bold values are for PNe in the Sagittarius dwarf galaxy (Dudziak et al. 2000).

⁵ B, Bule subset B; npc, non-photometric conditions; hbt, high brightness temperature, $T_b > 10000$ K; lrf, low radio flux, $S_\nu < 10$ mJy.

4: PNE FLUX DETERMINATIONS